doi: 10.4149/gpb_2024031

Cytotoxic and pro-oxidant profile of a photosensitive ruthenium nitrosyl candidate for NO delivery in healthy human fibroblasts

Hande Özbaşak[1,2], Hani M. Elbeheiry[3,4], Martin Schulz[3,5] and Lucia Račková[2,6]

[1] *Centre of Biosciences, Institute of Molecular Physiology and Genetics, Slovak Academy of Sciences, Bratislava, Slovakia*
[2] *Centre of Experimental Medicine, Slovak Academy of Sciences, Institute of Experimental Pharmacology and Toxicology, Bratislava, Slovakia*
[3] *Institute of Physical Chemistry, Friedrich Schiller University Jena, Jena, Germany*
[4] *Department of Chemistry, Faculty of Science, Damietta University, Egypt*
[5] *Department Functional Interfaces, Leibniz Institute of Photonic Technology, Jena, Germany*
[6] *Institute of Chemistry, Slovak Academy of Sciences, Bratislava, Slovakia*

Abstract. Ruthenium nitrosyl (Ru-NO) complexes are of interest as photoactive nitric oxide (NO) donor candidates for local therapeutic applications. NO plays a crucial regulatory role in skin homeostasis, concentration-dependently affecting processes like the proliferation, apoptosis, autophagy and redox balance. In this context, we investigated HE-10, a ruthenium-based photoinducible NO donor, for its pro-oxidant and cytotoxic effects under light and dark conditions in VH10 human foreskin fibroblast cells. We also tested its intracellular and extracellular NO-releasing function. Our study reveals a significant dose-dependent cytotoxic effect of HE-10, an increase in intracellular reactive oxygen and nitrogen species, and the occurrence of apoptosis in skin fibroblast cells. Furthermore, exposure to both increasing doses of HE-10 and white LED light led to substantial cellular events, including a significant induction of autophagy and G2/M phase cell cycle arrest. Paradoxically, these effects were not solely attributable to NO release based on DAF2-DA NO probe results, suggesting that intracellular photochemical reactions additional to NO photolysis contribute to biological activity. This study shows that HE-10 exhibits both cytotoxic and potential therapeutic effects, depending on concentration and light exposure. These findings are crucial for developing targeted Ru-NO complex treatments for skin diseases and potentially certain types of skin cancer, where controlled NO release could be beneficial.

Key words: Photosensitive nitric oxide donor — Ruthenium nitrosyl complex — Cytotoxicity — Oxidative stress — Skin fibroblasts

Introduction

The skin, our body's largest organ, is essential for overall health and well-being, acting as a protective barrier, regulating body temperature, and playing a key role in sensory perception (Honari 2017). Maintaining skin health involves a delicate balance of physiological, structural, and functional processes, collectively known as skin homeostasis (Wagner et al. 2021).

Nitric oxide (NO) is a versatile and crucial signaling molecule in the human body, playing a key role in various physiological processes, including regulating blood flow, immune response, and neural communication (Dusting 1995; Guzik et al. 2003; Calabrese et al. 2007). In skin homeostasis, NO serves as a key regulator of multiple physiological processes affecting cell growth, differentiation and apoptosis. Various skin cells, including fibroblasts, endothelial cells, keratino-

Correspondence to: Hande Özbaşak, Centre of Biosciences, Institute of Molecular Physiology and Genetics, Slovak Academy of Sciences, Dúbravská cesta 9, 840 05 Bratislava, Slovakia
E-mail: hande.celik93@gmail.com

© The Authors 2024. This is an **open access** article under the terms of the Creative Commons Attribution-NonCommercial 4.0 International License (https://creativecommons.org/licenses/by-nc/4.0/), which permits non-commercial use, distribution, and reproduction in any medium, provided the original work is properly cited.

cytes and immune cells, produce NO, which contributes to its multifaceted role in skin biology (Man et al. 2022; Kim and Choi 2023). Its multifaceted role in skin biology extends to vasodilation, melanogenesis, and immune responses, while also contributing to both protective and potentially harmful effects depending on its concentration and cellular context (Bruch-Gerharz et al. 1998). Recent studies have further elucidated NO's involvement in wound healing, vascular homeostasis in the skin (Suschek et al. 2022). Additionally, it plays a crucial role in managing skin inflammation, antimicrobial defense and various skin diseases and disorders (Kajiya et al. 2008; Mowbray et al. 2009).

Skin fibroblasts are vital cells in the dermis that produce the extracellular matrix and aid in wound healing (Stunova and Vistejnova 2018). These cells interact closely with NO in ways that are becoming increasingly important for dermatological research. Fibroblasts both produce and respond to NO, creating a complex signaling network in the skin (Tobin 2017). Notably, the unique ability of them to produce NO makes a significant contribution to the skin's defense mechanism (Lavnikova and Laskin 1995).

The antibacterial properties of metal-containing compounds have emerged as promising candidates for wound healing applications and photodynamic therapy, especially when dealing with multi-drug-resistant pathogens (Yaşayan et al. 2023). Recent studies in dermatology have focused on the potential of NO donors, including photoactivated ruthenium nitrosyl (Ru-NO) complexes, for wound healing, treatment of chronic skin conditions, and diabetic ulceration (Weller 2003; Walton et al. 2019; Elbeheiry and Schulz 2024). These complexes offer controlled NO delivery in skin applications by releasing NO on demand when exposed to light (Kumar et al. 2018), with Ru(ptp)(o-bqdi)NO_3-type complexes showing high NO release quantum yields under visible white LED light irradiation (Rose and Mascharak 2008). Ru-NO complexes have demonstrated promise in improving NO stability in the skin (Marquele-Oliveira et al. 2010) and exhibit satisfactory performance in releasing and preserving NO from degradation *in vitro*, making them promising vehicles for topical NO delivery (de Lima et al. 2017).

Recent advances have further highlighted their potential as controlled NO-release agents for various biomedical applications, including cancer therapy and antimicrobial treatments, with particular progress in developing light-activated NO donors sensitive to wavelengths within the therapeutic window (Stepanenko et al. 2022; Bhowmik and Roy 2024; Singh et al. 2024). The controlled release of NO through light activation could provide a targeted approach to managing skin conditions while minimizing potential side effects. However, recent advances in the field of ruthenium (Ru)-based photoactivated chemotherapy (PACT) have revealed that the biological effects of these compounds are not solely due to NO release. Instead, they involve a complex interplay of photosubstitution reactions, release of bioactive ligands, generation of reactive oxygen species (ROS), and interactions with cellular components. At lower concentrations, they could provide beneficial NO release for treating chronic wounds or inflammatory disorders, while at higher concentrations, their cytotoxic effects could be harnessed for conditions like actinic keratosis or localized skin cancers (Bonnet 2023).

This study aims to investigate the NO-releasing properties, pro-oxidant and cytotoxic effects of [Ru(ptp)(o-bqdi)NO]$(PF_6)_3$] (HE-10), on healthy VH10 human foreskin fibroblast cells under both light and dark conditions. By examining HE-10's effects on VH10 fibroblast cells, we sought to evaluate its potential as a NO donor candidate for dermatological applications and guide future research on its therapeutic use in skin diseases.

Material and Methods

Chemicals

All reagents used were of the highest analytical purity and quality. Dulbecco's modified Eagle medium (DMEM), fetal bovine serum (FBS), glutamine, penicillin/streptomycin, and 0.05% Trypsin/EDTA were obtained from Lonza (Belgium). 3-(4,5-Dimethylthiazol-2-yl)-2,5-diphenyltetrazolium bromide (MTT), acridine orange (AO), ethidium bromide (EB), dimethyl sulfoxide (DMSO), sodium dodecyl sulfate (SDS), phenylmethylsulfonyl fluoride (PMSF), bovine serum albumin (BSA), phosphate buffered saline (PBS), propidium iodide (PI), RNase, Triton-X, 2',7'-dichlorodihydr ofluorescein diacetate (H_2DCF-DA), 4,5-diaminofluorescein diacetate (DAF-2 DA), and other chemicals were purchased from Sigma Aldrich (Missouri, USA), unless otherwise stated. Rabbit monoclonal antibodies to PSMB-5, p21 Waf1/Cip1, LC3A/B, and β-actin were purchased from Cell Signaling Technologies, Inc. (Massachusetts, USA). Bradford assay was purchased from Bio-Rad (California, USA). Nitrocellulose membranes (sc-201699) and Western blotting luminol reagent (sc-2048) was acquired from Santa Cruz Biotechnology Inc. (Texas, USA).

Ru-NO donor [Ru(II)(ptp)(o-bqdi)NO]$(PF_6)_3$ HE-10

Synthesis: The ruthenium (II) nitrosyl-complex incorporating 4'-phenyl-terpyridine and benzoquinone diimine, [Ru(ptp)(o-bqdi)NO]$(PF_6)_3$] (HE-10), was synthesized as follows. The ptp ligand was prepared following the reported literature procedure (Dai et al. 2021). Complex HE-10 (Fig. 1) was synthesized following the synthetic route in references (de Lima et al. 2006; Shi et al. 2019).

Characterization: Yield 253 mg (92 %); FTIR ν (cm^{-1}): 1890 (N–O); ^{1}H NMR (400MHz, DMSO-d_6, 24°C) δ (ppm): δ 9.32 (s, 2H), 9.25–9.06 (m, 3H), 8.53 (d, J = 8.8 Hz, 4H), 8.41–8.24 (m, 4H), 8.23 (s, 1H), 8.09 (d, J = 5.2 Hz, 2H), 7.78 (s, 2H), 7.58 (d, J = 8.2 Hz, 3H); MS-ESI-positive (m/z): 695.03 ($[M–2PF_6^- +3H]^+$), calculated 695.07.

NO release measurements: NO release in solution was monitored *via* amperometric detection using an ISO-NOmeter NO-electrode (World Precision Instrument). The system had a short response time < 5 seconds and a sensitivity range of 1 nM to 20 µM. Sensor calibration was performed using standard solutions of sodium nitrite with 0.1 M sulfuric acid and 0.01 M potassium iodide.

Irradiation experiments were conducted in a quartz cuvette (1 cm path length, 3 ml capacity) using a 365 nm LED (35 mW). To prevent photoelectric interference, the electrode was positioned outside the light path. The solution was continuously stirred during measurements.

UV spectroscopy: Time-lapse UV-vis spectra were recorded on a J Jasco V-780 spectrometer, with a custom-built thermostated cell holder. Samples in a 10×10 mm quartz cuvette were irradiated with collimated beams from LEDs at 365 nm (M365LP1), 420 nm (M420L3), 455 nm (M455L3), or 505 nm (M505L3). All LED lamps were procured from Thorlabs Inc. The radiant power was measured using a thermopile sensor (LM-10 HDT, Coherent).

HE-10 stock solutions were prepared in DMSO (Sigma Aldrich) under dark conditions and stored at −80°C until use.

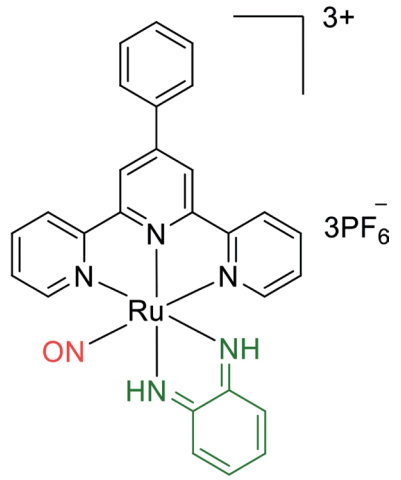

HE-10

Figure 1. Chemical structure of the $[Ru(ptp)(o\text{-}bqdi)NO](PF_6)_3$ complex HE-10.

Experimental workflow and light irradiation of HE-10

To activate the HE-10 complex and induce NO release, we exposed VH10 fibroblast cells directly to a visible white LED lamp. The irradiation experiments utilized a visible white LED light source with a power of 6 W, color temperature of 4200 K, and an irradiance of 20 mW/cm^2 (ChiliTec GmbH, Germany). In all experiments, the VH10 fibroblasts were illuminated for 1 hour. The light source was positioned 5 cm above the cell culture plates, illuminating them from above. This setup remained consistent across all experiments involving light activation of the HE-10 complex.

Cell culture and treatment

VH10 human foreskin fibroblast cells, were obtained from Dr. Horvathova at the Cancer Research Institute of Slovak Academy of Sciences, were grown and maintained as previously described at 37°C under a 5% CO_2 atmosphere (Csekes et al. 2020). VH10 fibroblasts were not used beyond the 20th passage in any experiment.

HE-10 treatment solutions were freshly prepared in cell media prior to cell treatment, with the final DMSO concentration in the cell culture medium not exceeding 0.5% (v/v). The experimental groups were divided into two groups: Light and Dark. The light group was exposed to white LED light for 1 hour to activate the HE-10 compound, while the dark group was kept under the same conditions without light exposure. Following the 1-hour treatment, all groups were incubated for an additional 17 hours in dark conditions.

MTT assay for cell viability

The cytotoxicity of HE-10 complex (0–15 µM) was assessed using the MTT assay. VH10 fibroblasts were seeded at 7000 cells *per* well in 96-well plates. After 18 hours of treatment with HE-10 under light or dark conditions, cells were incubated with 0.5 mg/ml MTT in cell medium for 2 hours at 37°C and 5% CO_2. The formazan crystals were then solubilized by adding 100 µl of 10% SDS in 0.01 M HCl. Absorbance was measured at 570 nm with a 690 nm reference using a TECAN Infinite F200 microplate reader. The 50% inhibitory concentration (IC_{50}) values were calculated using GraphPad Prism 9.

Acridine orange-ethidium bromide staining

VH10 fibroblasts were seeded in 24-well plates and cultured for 24 hours before treatment with 3, 4.5, 7.5, and 9 µM HE-10 in fresh cell medium under light or dark conditions. Cells were then incubated with cell medium containing 10 µg/ml AO, and 10 µg/ml EB for 20 min at 37°C and 5% CO_2 atmosphere. Stained cells were observed using a fluorescence microscope (Leica DM IL LED, Germany).

Griess assay

VH10 fibroblasts were treated with HE-10 complex as described above. After treatment, 100 µl of culture media was collected from each wells and mixed 1:1 with Griess reagent (0.5% sulphanilamide, 0.05% naphthyl ethylenediamine dihydrochloride in 2.5% phosphoric acid). A standard curve was generated using 0–50 µM $NaNO_2$. Absorbance was measured at 540 nm with a 690 nm reference using a microplate reader (Infinite M200, TECAN, Switzerland).

Western blotting

VH10 fibroblasts were seeded at a density of 210,000 cells *per* well in 6-well plates and grown for 24 hours. The cells were then treated with the indicated HE-10 concentrations in 5% CO_2 at 37°C for 18 hours. Following treatment, cells were washed with PBS and detached using 0.05% Trypsin/EDTA. After that, the cells were centrifuged at 14,000 × *g* for 1 min, at 4°C.

For protein extraction, cell pellets were resuspended with 1× cell lysis buffer (stock 10×), containing 1 mM PMSF and 0.1% (v/v) SDS. The cells were homogenized with lysis buffer for 20 min on ice, briefly vortexing every 5 min. Following homogenization, the lysates were centrifuged at 14,000 × *g* for 30 min, at 4°C. The supernatant was collected and kept on ice and the total protein concentrations were measured using the Bradford assay.

Prior to electrophoresis, proteins were denatured by heating at 96°C for 5 min in Laemmli buffer. The proteins were then separated by SDS-polyacrylamide gel electrophoresis using a Mini PROTEAN Tetra Cell system with a PowerPac HC Power Supply (Bio-Rad). After separation, proteins were transferred to nitrocellulose membranes.

Membranes were blocked with 3% BSA in PBS-T (PBS with 0.1% (v/v) Tween-20, Merck) for 2 hours. Following blocking, membranes were incubated overnight at 4°C with primary antibodies against PSMB-5 (#12919), p21 Waf1/Cip1(#2947), LC3A/B (#12741), and β-actin (#4970). After primary antibody incubation, membranes were rinsed several times with PBS-T before incubating with appropriate secondary antibodies. Protein bands were detected using a luminol reagent. Densitometric measurements of the protein bands were carried out using ImageJ software.

Cell cycle analysis with flow cytometry

VH10 cells were treated with HE-10 complex as described above. Following treatment, cells were washed with PBS, detached using trypsin, and centrifuged at 2000 × *g* for 2 min. The cells pellets were then fixed in 70% ethanol at −20°C until pellet formation was observed which typically took approximately one week.

After fixation, the cells were centrifuged at 2000 × *g* for 2 min, washed with cold PBS, and incubated on ice for 10 min. PI staining solution containing 10 mg/ml PI, 100 µg/ml RNase, and 0.1% (v/v) Triton-X was prepared and kept on ice. The cell pellets were then resuspended in this PI staining solution and incubated for 15 min at 37°C in a 5% CO_2 atmosphere.

Cell cycle phase distribution was analyzed using a flow cytometer (FC500, Beckman Coulter). Data analysis was performed using CXP Analysis software (Beckman Coulter), with a minimum of 5,000 cells analyzed *per* sample. To differentiate between debris and intact cells, gates were set on a forward scatter *versus* side scatter dot plot. The percentage of cells in each cell cycle phase (G0/1, S, and G2/M) was determined based on the gated populations and used for statistical analysis.

Reactive oxygen and nitrogen species (RONS) measurement with H_2DCF-DA probe

RONS levels induced by HE-10 were assessed using the H_2DCF-DA probe. VH10 cells, cultured overnight in 6-well plates, were treated with HE-10 complex at previously described concentrations. Cells were then stained with 10 µM H_2DCF-DA for 40 min at 37°C in 5% CO_2 atmosphere. After staining, cells were washed with PBS, trypsinized, and centrifuged at 2000 × *g* for 2 min. The cell pellets were resuspended in cold PBS, and fluorescence intensity was measured *via* flow cytometry, analyzing 10,000 cells *per* sample. Data were analysed using CXP Analysis software.

Intracellular NO measurement with DAF2-DA probe

Intracellular NO levels were measured using DAF2-DA probe. VH10 cells were cultured overnight in 6-well plates, and treated with HE-10 at indicated concentrations for 1 hour. Cells were then stained with 10 µM DAF2-DA for 40 min at 37°C in a 5% CO_2. After washing with PBS, cells were trypsinized, centrifuged at 2000 × *g* for 2 min, and resuspended in cold PBS. Fluorescence intensity was measured by flow cytometry, analyzing 10,000 cells *per* sample. Data were analysed *via* CXP Analysis software.

Statistical analysis

Statistical analysis was performed using GraphPad Prism software (version 9), and all data were expressed as mean ± SEM. A two-way ANOVA was conducted to assess the effects of HE-10 concentration, light exposure and the interaction between them on the measured outcomes. The two-way ANOVA followed by Bonferroni *post hoc* tests, was used to compare light and dark groups. Additionally,

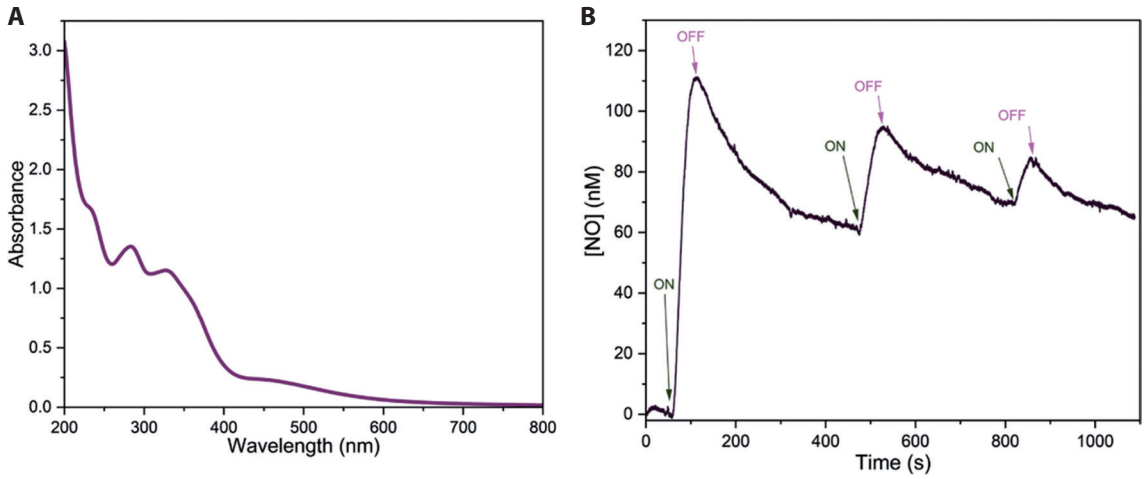

Figure 2. A. UV-visible spectra of the complex HE-10 in acetonitrile (30 μM). **B.** Amperometrically detected NO-release profile of HE-10 (30 μM) in acetonitrile observed upon irradiation with 365 nm LED (35 mW). The LED on/off cycles showcase the light dependence of NO-release.

Dunnett's multiple comparisons test was used to compare each experimental group with its respective control. All data were analyzed for homogeneity of variance using the Brown-Forsythe test. The assumption of equal variances was met, affirming the validity of the ANOVA model.

Results

HE-10 synthesis and characterization

The synthesis of complex HE-10 was carried out following the previously reported procedure for preparing similar complexes (Shi et al. 2019). The ptp ligand was reacted with ruthenium(III) chloride hydrate to produce the trichlorido complex, which was then reacted with o-bqdi in the presence of triethylamine to yield the monochlorido complex. The chlorido ligand was then replaced by a nitrito ligand, which was eventually converted to a nitrosyl ligand by a strong acid. HE-10 was characterized by nuclear magnetic resonance (NMR), mass spectrometry (MS), and infrared spectroscopy (IR), which indicate a diamagnetic complex that can be represented as Ru(II)(NO+), as expected. The presence of the nitrosyl ligand is confirmed by the absorption band at 1890 cm^{-1} in the IR spectrum and is indicative of the linear binding fashion of the nitrosyl group (De La Cruz and Sheppard 2011). The UV-visible spectrum of HE-10 shows two maxima absorption peaks, one at 331 nm (ε = 27953 $M^{-1}cm^{-1}$) and the second at 278 nm (ε = 31810 $M^{-1}cm^{-1}$) due to metal-to-ligand charge transfer (MLCT) and ligand-centered (LC) transitions (Fig. 2A). In addition, there is a weak broad band from 420 nm to 600 nm (ε = 2571 to 7602 $M^{-1}cm^{-1}$).

NO-photorelease in solution

HE-10 released NO when irradiated with low-power LEDs with different wavelengths, and the released NO in solution was quantified with an electrochemical NO-sensor (Fig. 2B). The time-dependent evolution of NO release was monitored by UV-visible absorption spectra under irradiation with 365, 420, 455, and 505 nm LEDs in acetonitrile (Fig. 3). Upon irradiation of HE-10, the formation of the Ru(III) photoproduct can be followed by the increase of the absorption bands at 282 nm and 310 nm and a new broad transition band centered at 511 nm (Works and Ford 2000; Fry et al. 2011). Moreover, the presence of three isosbestic points at 270, 322, and 400 nm indicates the clean conversion of HE-10 to the photoproduct during NO release. Upon irradiation at 365, 420, and 455 nm, most NO is released within the first 30 min of irradiation (Fig. 3A,B,C). Irradiation at 505 nm is slower because the photoproduct absorbs at the irradiation wavelength (Fig. 3D). Control experiments in the dark confirmed the light dependence of the NO release reaction. The quantum yields for NO-photorelease reaction were estimated according to a reported method (Stadler et al. 2018). The quantum yield values are summarized in Table 1.

Effects of HE-10 on cell viability in light and dark conditions

Our study investigated the effects of the Ru-NO complex HE-10 on VH10 human fibroblast cells under light and dark conditions. We observed a dose-dependent decline in cell viability following HE-10 treatment, with a significantly enhanced effect under light exposure conditions (Fig. 4A). The IC_{50} value of HE-10 was 9.20 ± 0.40 μM under light

Table 1. Quantum yields (φ_{NO}) for photochemical NO release from HE-10 at different irradiation wavelengths at 25°C (λ_{LED})

λ_{LED} (nm)	Quantum yield
365	4.59×10^{-3}
420	1.70×10^{-3}
455	7.90×10^{-4}
505	6.14×10^{-4}

conditions and 11.12 ± 0.50 μM in the dark, indicating increased potency with light exposure.

The outcomes were significantly influenced by both the interaction of HE-10 concentration and light exposure ($F(8, 36) = 2.936$, $p = 0.0124$), and each factor independently. HE-10 concentration ($F(8, 36) = 149.5$, $p < 0.0001$) and light exposure ($F(1, 36) = 17.78$, $p = 0.0002$) both showed significant effects in the two-way ANOVA analysis. A minor decrease in cell viability compared to the control was observed starting from the 4.5 μM dose (* $p \leq 0.05$). In the light-exposed group, doses of 6 and 7.5 μM demonstrated highly significant (*** $p \leq 0.001$), while in the dark group, the same doses showed significant effects (** $p \leq 0.01$) compared to controls. At 9 μM, the light-exposed group exhibited a more pronounced decrease in cell viability (**** $p \leq 0.0001$) than the dark group (*** $p \leq 0.001$). Doses ranging from 10.5 to 15 μM led to substantial reductions in cell viability in both groups (**** $p \leq 0.0001$) compared to controls. Notably, at 10.5 μM (#### $p \leq 0.0001$), a clear difference in cell survival was observed between the light and dark group (Fig. 4A). Moreover, at 9 μM, only light-exposed cells showed a viability decrease below 70%, which is considered the threshold for the non-cytotoxic effects (Thangaraju and Varthya 2022). Based on these results, we selected doses of 3, 4.5, 7.5, and 9 μM for subsequent experiments.

Morphological changes were assessed using AO/EB dual staining (Fig. 4B). While control cells (0.5% DMSO) and those treated with 3 μM HE-10 maintained normal nuclear (green) and cytosolic structures (red-orange), cells exposed to 9 μM HE-10 under white LED light showed a higher

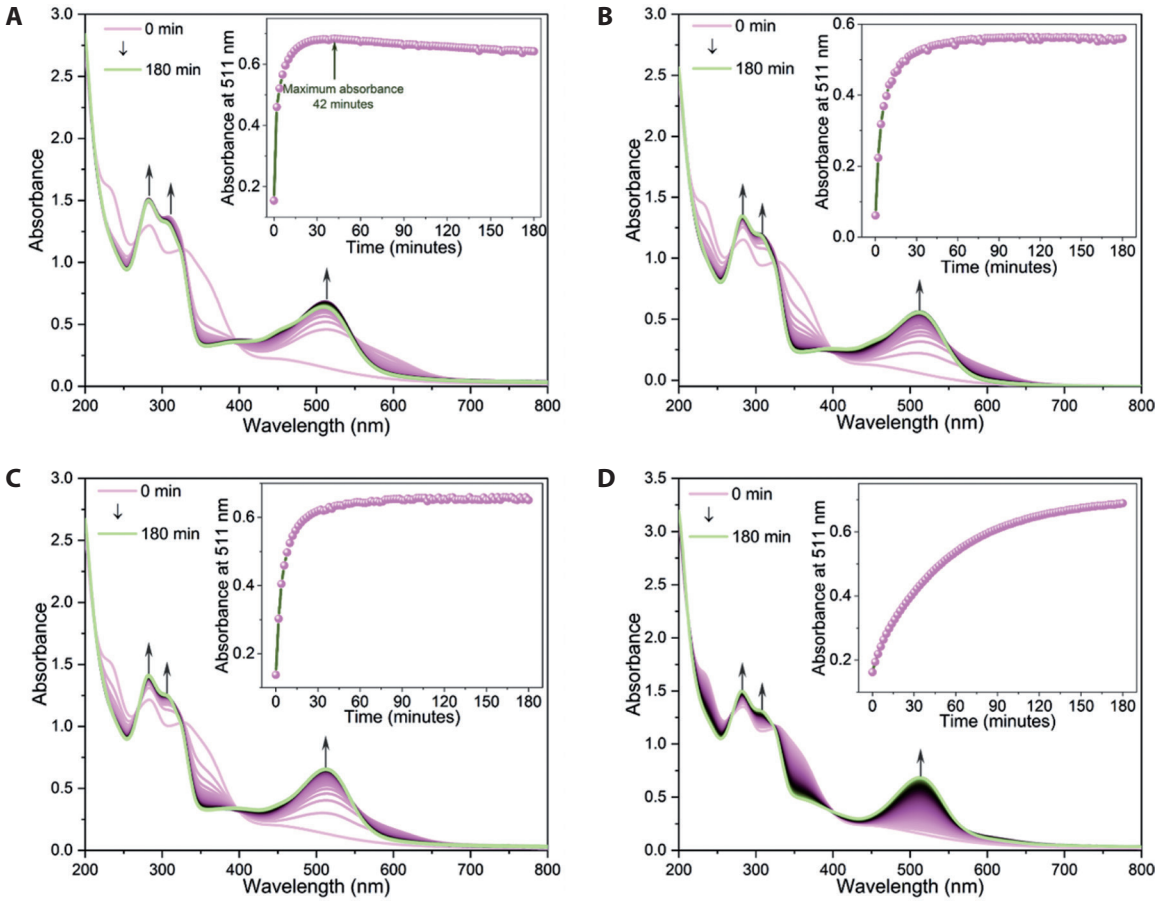

Figure 3. UV-visible spectra of HE-10 (30 μM) in acetonitrile with a 3-ml sample volume upon illumination with **A)** 365 nm LED (35 mW), **B)** 420 nm LED (99 mW), **C)** 455 nm LED (173 mW), **D)** 505 nm LED (32 mW) with a 2-min step for each recorded spectrum. Insets: the absorbance growth at 511 nm.

number of early and late apoptotic cells, corroborating the quantitative cell viability data.

Light exposure enhanced G2/M arrest by HE-10 in VH10 cell cycle progression

We assessed the influence of HE-10 on VH10 fibroblast cell cycle distribution by treating cells with various concentrations (3, 4.5, 7.5, and 9 μM) under light and dark conditions. Two-way ANOVA revealed significant effect of HE-10 concentration $F(4, 20) = 4.9505$, $p = 0.0064$, and light exposure, $F(1, 20) = 9.156$, $p = 0.0067$) on the G1 phase outcomes, without significant interaction between these factors. There were no significant pairwise differences between light and dark groups. Light-exposed 7.5 μM (* $p \leq 0.05$) and 9 μM (** $p \leq 0.01$) HE-10 concentrations showed a statistically significant decrease in the G1 phase (Fig. 5A).

For the S phase, light exposure alone was not statistically significant ($F(1, 20) = 2.61$, $p = 0.1220$). However, HE-10 concentrations significantly affected the S phase, accounting for 36.58% of the total variance ($F(4, 20) = 3.447$, $p = 0.0268$). Particularly, Dunnett's multiple comparisons test found a significant effect of 9 μM HE-10 on the S phase

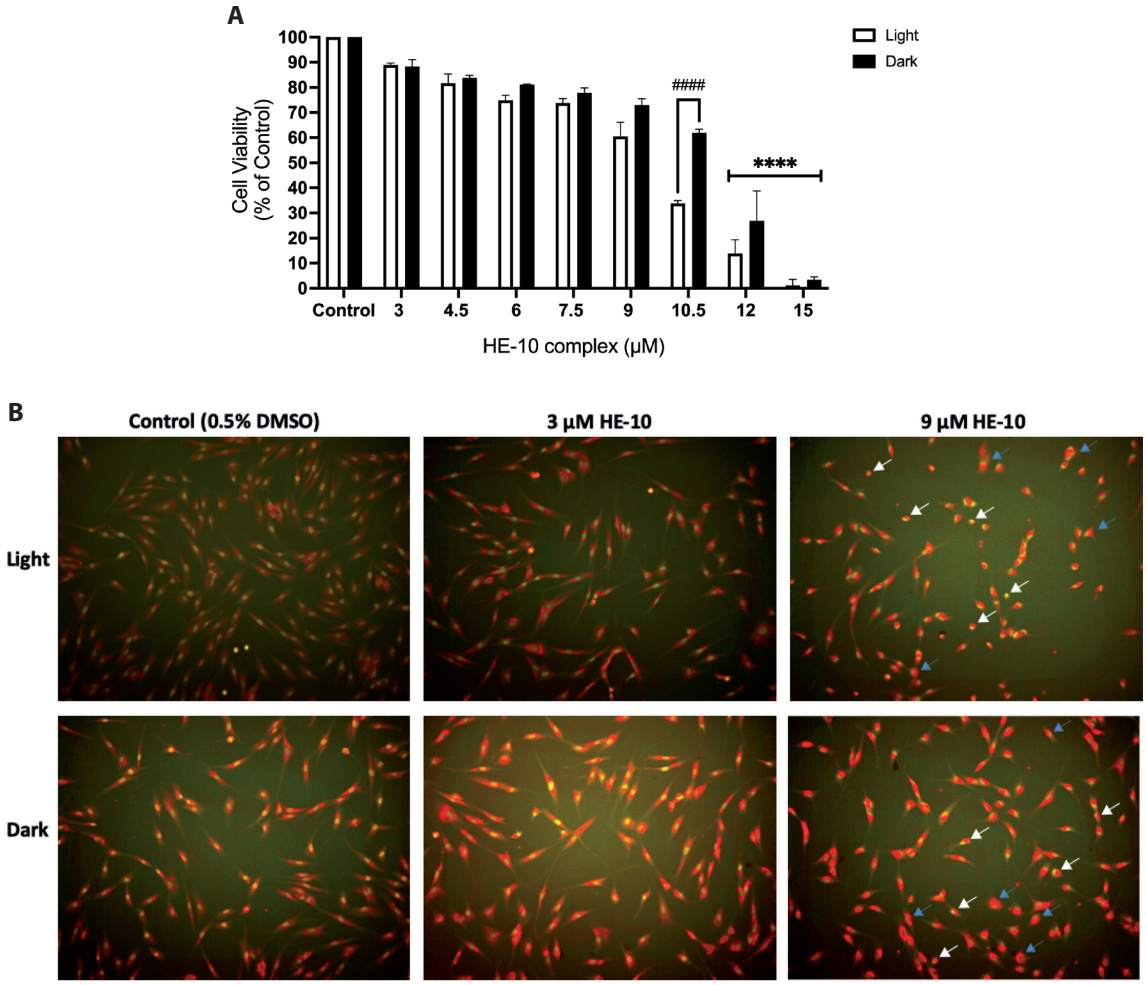

Figure 4. Viability of VH10 fibroblasts in response to HE-10 treatment under light and dark conditions. **A.** VH10 fibroblasts were seeded at 7,000 cells *per* well. After 24 hours, cells were treated with various concentrations of HE-10, ranging from 3 μM to 15 μM, with the control wells receiving 0.5% DMSO. Immediately after adding the HE-10 compound to the fresh cell medium, the cells were either exposed to 1 hour of light or maintained in darkness. Subsequently, all cells were incubated in darkness for 17 hours in a CO_2 incubator. The IC_{50} value of HE-10 was 9.20 ± 0.40 μM under light conditions and 11.12 ± 0.50 μM in the dark. Data represent mean ± SEM ($n = 3$). Two-way ANOVA with Bonferroni's multiple comparisons test; $^{\#\#\#\#}$ $p \leq 0.0001$ *vs.* the same treatment w/o light, and Dunnett's multiple comparisons test; * $p \leq 0.05$, ** $p \leq 0.01$, *** $p \leq 0.001$, **** $p \leq 0.0001$ *vs.* control. **B.** Fluorescence microscopy images of AO/EB staining on VH10 cells. The blue arrows indicate cells in early apoptosis, while the white arrows indicate cells in late apoptosis. Magnification: 10×, $n = 2$. (For color figure see online version of the manuscript.)

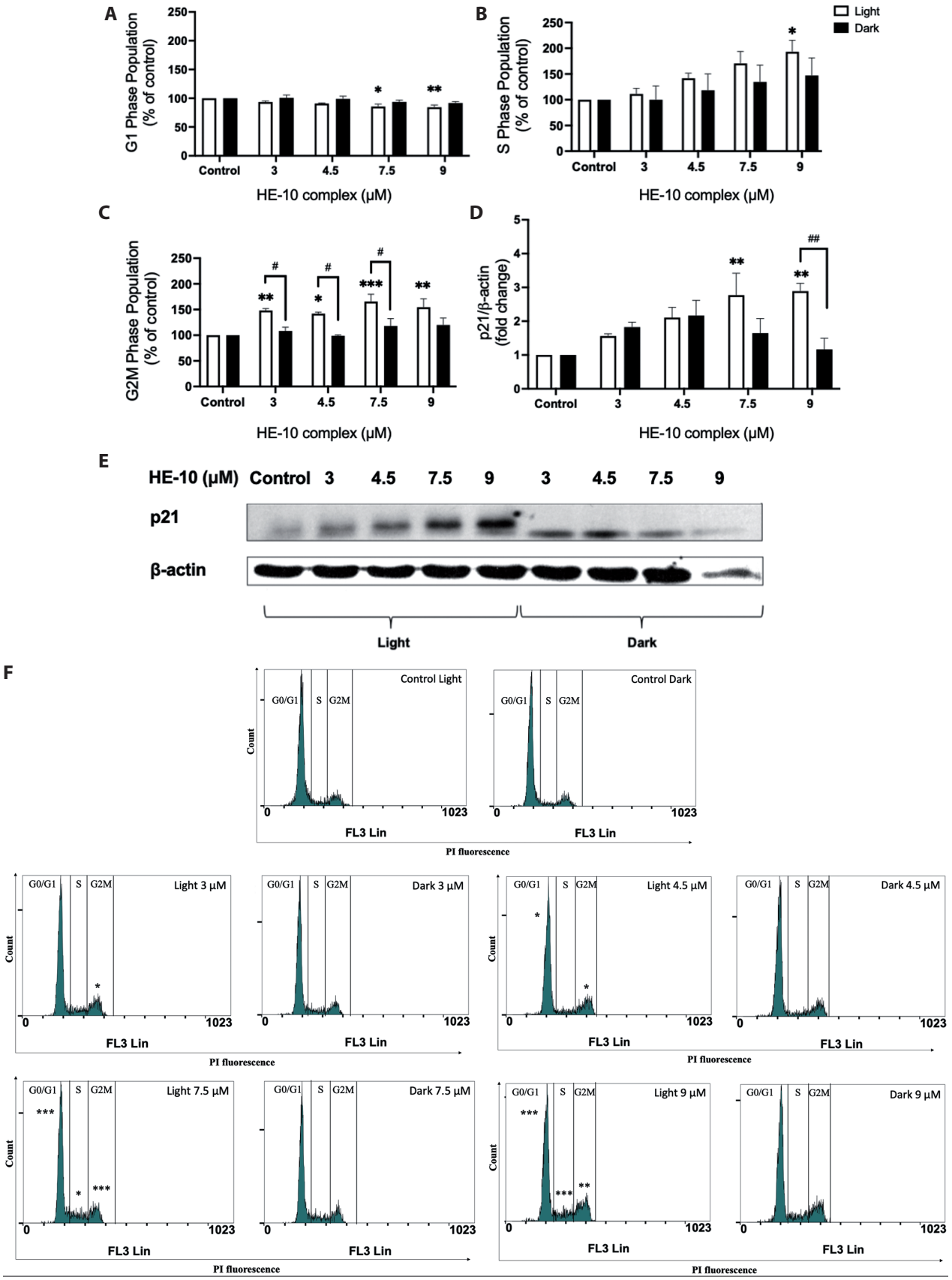
A
G1 Phase Population (% of control)
HE-10 complex (µM)
Control
3
4.5
7.5
9
B
S Phase Population (% of control)
Light
Dark
C
G2M Phase Population (% of control)
D
p21/β-actin (fold change)
E
HE-10 (µM) Control 3 4.5 7.5 9 3 4.5 7.5 9
p21
β-actin
Light
Dark
F
Control Light
Control Dark
Light 3 µM
Dark 3 µM
Light 4.5 µM
Dark 4.5 µM
Light 7.5 µM
Dark 7.5 µM
Light 9 µM
Dark 9 µM
G0/G1
S
G2M
Count
FL3 Lin
PI fluorescence

◂ **Figure 5.** G2/M arrest and p21 upregulation after treatment with light-exposed HE-10. **A–C.** Quantitative analysis of cell cycle distribution in VH10 cells. **D.** p21 protein levels from VH10 cells were determined by Western blot. Quantification of p21 protein levels relative to β-actin. **E.** Representative images of the blot. Data were normalized by β-actin levels and expressed as fold changes ($n = 3$). **F.** Representative DNA frequency histograms, obtained by flow cytometry with propidium iodide DNA staining, show the percentage of cells in G1 (A), S (B), and G2/M (C) phases after treatment with various concentrations of HE-10 under both light and dark conditions. Results are presented as a percentage of all obtained events ($n = 3$). Data represent the mean ± SEM. Two-way ANOVA with Bonferroni's multiple comparisons test; $^{\#}$ $p \leq 0.05$, $^{\#\#}$ $p \leq 0.01$ *vs.* the same treatment w/o light, and Dunnett's multiple comparisons test; * $p \leq 0.05$, ** $p \leq 0.01$, *** $p \leq 0.001$ *vs.* control (0.5% DMSO).

under light (* $p \leq 0.05$) but not at lower concentrations or in darkness (Fig. 5B).

Both light exposure and HE-10 concentration independently affected the G2/M phase distribution (Fig. 5C). Light exposure accounted for 36.40% of the variance ($F(1, 20) = 29.02$, $p < 0.0001$), while HE-10 concentration was responsible for 28.81% ($F(4, 20) = 5.741$, $p = 0.0030$). On the other hand, there was no significant interaction effect between light exposure and HE-10 concentration ($F(4, 20) = 1.931$, $p = 0.1445$). Under light conditions, we observed a significant increase at all tested concentrations compared to the control: 3 μM (** $p \leq 0.01$), 4.5 μM (* $p \leq 0.05$), 7.5 μM (*** $p \leq 0.001$), and 9 μM (** $p \leq 0.01$). Comparisons of light *vs.* dark conditions showed significant increases at 3, 4.5, and 7.5 μM concentrations ($^{\#}$ $p \leq 0.05$; p-values of 0.0421, 0.0261, and 0.0122, respectively), but not at 9 μM ($p = 0.1015$, Fig. 5C).

We also assessed changes in p21 protein expression, which plays a key role in G2/M transition regulation. Two-way ANOVA revealed significant interactions between HE-10 concentration and light exposure ($F(4, 20) = 3.456$, $p = 0.0266$), with significant effects of the concentration ($F(4, 20) = 4.477$, $p = 0.0096$), and light exposure ($F(1, 20) = 5.818$, $p = 0.0256$) on p21 protein levels. Consistent with G2/M phase arrest of the cell cycle, we found a remarkable overexpression of p21 protein levels (Fig. 5D,E) in HE-10 groups exposed to 7.5 μM and 9 μM light relative to control levels (** $p \leq 0.01$), with a significant difference between light and dark groups at 9 μM ($^{\#\#}$ $p \leq 0.01$). Figure 5F shows representative DNA frequency histograms obtained by flow cytometry with PI staining.

These findings collectively suggest that both white LED light exposure and HE-10-mediated NO release cause DNA damage triggering G2/M arrest, depending on HE-10 concentration. Higher concentrations inhibit proliferation and induce cell cycle arrest in both G2/M and S phases.

Light irradiation increased extracellular NO release from HE-10 complex

The Griess assay results demonstrate that light exposure significantly enhanced nitrite levels in the cell culture medium of HE-10-treated VH10 fibroblasts (Fig. 6). Two-way ANOVA revealed a significant interaction between HE-10 concentration and light ($F(4, 20) = 3.123$, $p = 0.0378$), with significant main effects of the concentration ($F(4, 20) = 125.5$, $p < 0.0001$) and light exposure ($F(1, 20) = 43.31$, $p < 0.0001$). Nitrite levels, expressed as fold change relative to the control, were consistently higher in light conditions across all tested concentrations. For 4.5 μM, 7.5 μM, and 9 μM concentrations, light-exposed samples showed significantly higher nitrite levels than those kept in the darkness ($^{\#\#}$ $p \leq 0.01$). All tested HE-10 concentrations significantly increased nitrite levels compared to the control under both light and dark conditions (**** $p < 0.0001$).

HE-10 induces autophagy without affecting proteasomal activity

Disrupted proteostasis, characterized by the accumulation of damaged proteins, can lead to cellular malfunction and disease. To combat this, cells have evolved sophisticated mechanisms for protein degradation, primarily through the ubiquitin-proteasome system (UPS) and the autophagy-lysosome pathway. Both pathways are crucial for maintaining cellular health during aging (Ji and Kwon 2017). To investigate the impact of HE-10 on VH10 cells, we conducted

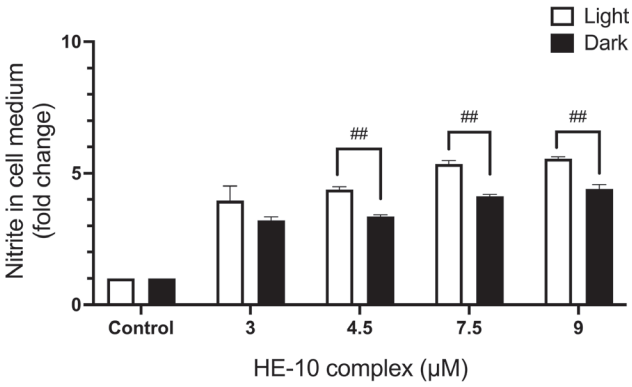

Figure 6. The effect of HE-10 on extracellular NO release under light or dark conditions. The bar graph shows the fold change in nitrite concentration in the cell culture medium of HE-10-treated cells (at 3, 4.5, 7.5 and 9 μM) compared to the control (0.5% DMSO). Data represent the mean ± SEM ($n = 3$) and are expressed as a fold change. Two-way ANOVA with Bonferroni's multiple comparisons test; $^{\#\#}$ $p \leq 0.01$ *vs.* the same treatment w/o light, and Dunnett's multiple comparisons test; **** $p \leq 0.0001$ vs. control.

Western blot analysis targeting two specific markers: PSMB5 for proteasome activity and LC3 for autophagy.

For the LC3II protein expression (Fig. 7A), the two-way ANOVA demonstrated a significant main effect of HE-10 concentration ($F(4, 20) = 4.045$, $p = 0.0146$). The interaction between concentration and light effect ($F(4, 20) = 1.872$, $p = 0.1548$), and the main effect of light ($F(1, 20) = 0.02923$, $p = 0.8660$) were not significant. Dunnett's multiple comparisons test highlighted a significant difference in LC3 expression when comparing control to 9 μM concentration under light conditions (** $p \leq 0.01$), while no significant differences were observed under dark conditions. At 9 μM under light conditions, LC3 expression was approximately 2.5-fold higher than control.

As shown in Figure 7B, PSMB5 expression showed no significant differences across all conditions tested. The levels remained relatively constant with HE-10 treatment ranging from 3 μM to 9 μM, both under light and dark conditions. This suggests that HE-10 treatment and light exposure do not influence the proteasomal degradation pathway. Representative images of the blots are presented in Figure 7C.

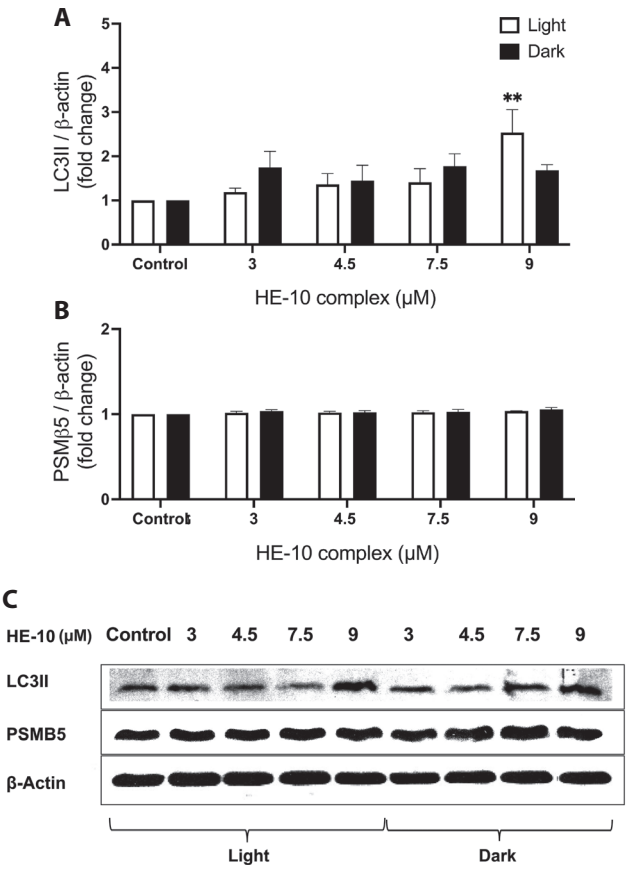

Figure 7. Effect of HE-10 on the proteins involved in autophagy and proteasomal degradation. Protein levels from VH10 cells were determined by Western blot. **A.** Quantification of autophagy marker LC3II. **B.** Proteasome beta 5 subunit (PSMB5) immunoblots. **C.** Representative images of the blots. Data were normalized to β-actin levels and expressed as fold-change. Data represent mean ± SEM ($n = 3$). Two-way ANOVA with Dunnett's multiple comparisons test; ** $p \leq 0.01$ *vs.* control (0.5% DMSO).

These findings indicate that HE-10 promotes autophagic activity in a light-dependent manner at higher concentrations, which could have implications for cellular homeostasis and survival under stress conditions. The data suggest a selective effect on autophagy without impacting proteasomal activity.

HE-10 induced RONS production under light and dark conditions

Controlled release of NO from Ru-NO complexes enhances cytotoxic effects by generating RONS when exposed to light (Shi et al. 2019). To investigate if HE-10-induced cell death is due to elevated RONS levels, we measured intracellular RONS levels in VH10 cells by flow cytometry using the H_2DCF-DA probe.

There was a highly significant main effect of HE-10 concentration ($F(4, 20) = 85.78$, $p < 0.0001$), while the interaction between light exposure and concentration ($F(4, 20) = 0.6328$, $p = 0.6449$) and the main effect of light exposure alone ($F(1, 20) = 3.400$, $p = 0.0801$) were not significant.

Representative histograms show the changes in 2',7'-dichlorofluorescein (DCF, the fluorescent product of H_2DCF-DA oxidation) mean fluorescence intensity (M.F.I.) among the control groups (0.5% DMSO) and the groups treated with 7.5 μM and 9 μM concentrations of HE-10 (Fig. 8A). Treatment with HE-10 for 18 hours significantly elevated RONS levels at higher concentrations in both light and dark conditions. Although there was a slight increase in DCF fluorescence intensity in the light-exposed groups, *post hoc* analysis showed these increases were not statistically significant between light and dark conditions across all concentrations. Only the 7.5 and 9 μM concentrations exhibited a significant difference from the control under both light and dark conditions (Fig. 8B, **** $p \leq 0.0001$).

These results suggest that HE-10 induces RONS production in a concentration-dependent manner, with minimal influence from light exposure under these experimental conditions.

Intracellular NO production in response to HE-10

Intracellular NO production in cells treated with HE-10 was measured using DAF-2 DA M.F.I. *via* flow cytometry. NO production was compared under light and dark conditions at non-toxic (3 μM) and cytotoxic (9 μM) HE-10 concentrations. Figure 9A shows histograms of DAF fluorescence M.F.I. obtained by measuring intracellular NO levels. Statistical analysis a two-way ANOVA indicated

a significant effect of HE-10 concentration on DAF M.F.I. ($F(2,12) = 8.436$, $p = 0.0052$), but no significant effect of light condition or interaction between factors. *Post hoc* analysis using Dunnett's test showed a significant increase in M.F.I. at 9 μM in darkness compared to control (** $p \leq 0.01$), while no significant differences were observed between light and dark conditions for any concentration. Unexpectedly, the light-exposed group did not show any significant increase. Although the DAF assay did not yield statistically significant results for light exposure, a mild increase in NO levels was observed even at 3 μM HE-10 (Fig. 9B). This finding is noteworthy as NO is known to exert physiological effects at low nanomolar concentrations, suggesting that even modest elevations in NO could significantly impact cellular functions (Cheung et al. 2012).

Discussion

This study aimed to investigate the effects of the Ru-NO complex HE-10 on human skin fibroblasts, with a focus on its potential as a photoactivated NO donor for dermatological applications. Our primary objectives were to assess the cytotoxicity, pro-oxidant properties, and cellular responses to HE-10 under both light and dark conditions. We employed a range of methodologies, including cell viability assays, flow cytometry and Western blotting to comprehensively evaluate HE-10's impact on skin fibroblast homeostasis. Our research sought to elucidate whether HE-10 could serve as an effective and controlled NO delivery system for potential use in skin treatments, while also examining its effects on key cellular processes such as the cell cycle, autophagy, and oxidative stress responses. The key findings of this study include a dose-dependent decline in cell viability following HE-10 treatment, with light enhancing cytotoxicity; induction of G2/M cell cycle arrest and upregulation of p21 expression, particularly under light exposure; increased intracellular RONS levels, independent of light conditions; promotion of autophagy, evidenced by increased LC3-II expression under light conditions at higher concentrations; and enhanced stable end products of NO under light exposure, while intracellular NO levels exhibited unexpected patterns. This study contributes to the growing body of research on metal-based NO donors and their potential therapeutic applications in dermatology.

We observed the dose-dependent decline in cell viability following HE-10 treatment, with light enhancing the cytotoxicity of the complex at quite a low concentration range. Still, the IC_{50} value of HE-10 was much higher than the IC_{50} we measured in VH10 cells for doxorubicin (0.66 ± 0.18mM) (Csekes et al. 2020). However, it was lower compared to other Ru-NO complexes reported in fibroblast cells (de Souza Gois et al. 2019; do Nascimento et al. 2019; Barbosa et al. 2023).

The significant upregulation of the autophagic marker LC3-II only under light conditions at a concentration of 9 μM points to a potential adaptive response to HE-10 and light-induced stress. This finding is particularly

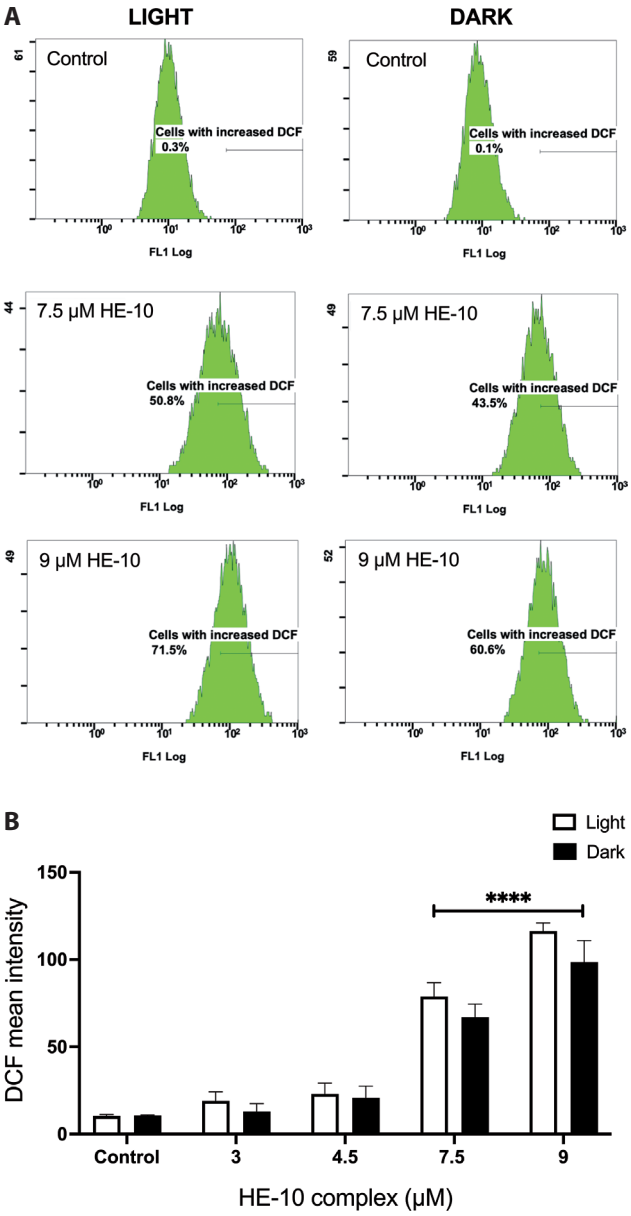

Figure 8. Pro-oxidant properties of HE-10 under light and dark conditions. VH10 cells were incubated with a range of HE-10 concentrations (3 to 9 μM), and RONS production was measured using the H_2DCF-DA probe *via* flow cytometry. **A.** Representative histograms display the changes in DCF M.F.I. among the control groups (0.5% DMSO) and the groups treated with 7.5 μM and 9 μM concentrations of HE-10. **B.** The bar graph shows RONS levels in the cells treated with HE-10 under light and dark conditions. Data represent mean ± SEM ($n = 3$). Two-way ANOVA with Dunnett's multiple comparisons test; **** $p \leq 0.0001$ *vs.* control.

interesting as it suggests that the complex may trigger cellular protective mechanisms, which could be beneficial in certain therapeutic contexts, such as promoting cellular resilience in aged or damaged skin. However, further research is needed to fully understand the implications of this autophagy induction and its potential therapeutic applications.

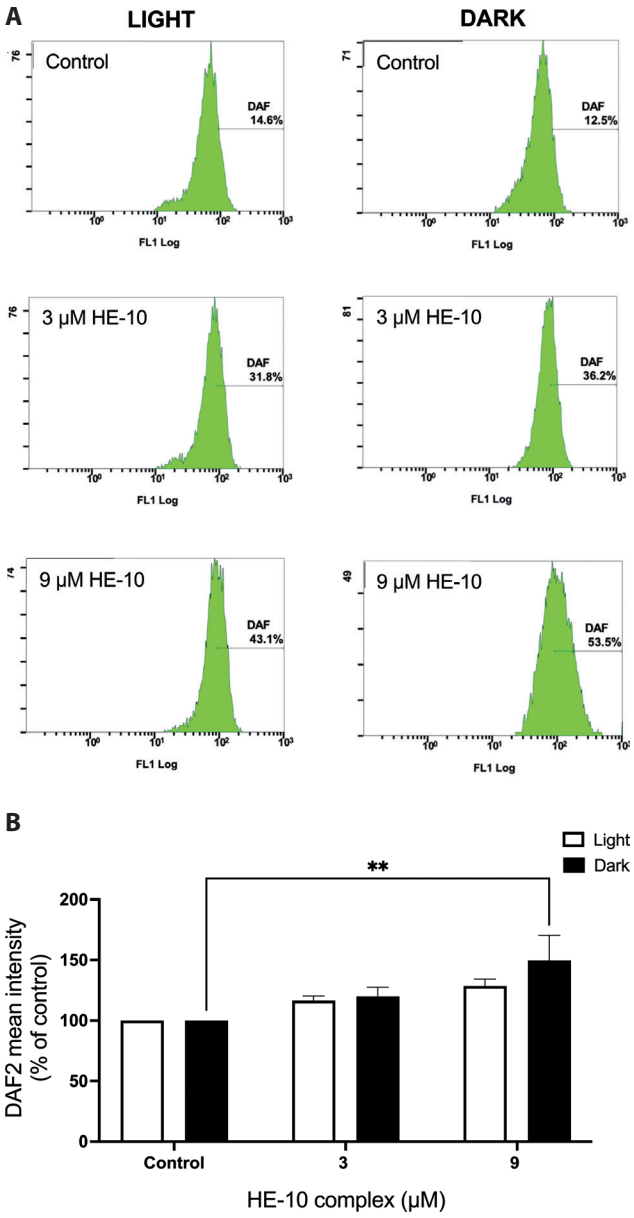

Figure 9. Intracellular NO production in cells treated with HE-10. Cells were treated with HE-10 at concentrations of 3 μM and 9 μM, with controls receiving 0.5% DMSO. Following HE-10 treatment, one group of cells was exposed to light for 1 hour, while the other group was kept in the dark. All cells were then incubated for 40 min with DAF-2 DA. **A.** Flow cytometry histograms showing DAF fluorescence M.F.I. of intracellular NO levels in cells treated with HE-10 under light and dark conditions. **B.** NO levels were quantified using DAF-2 DA M.F.I. by flow cytometry. Data represent mean ± SEM ($n = 3$). Two-way ANOVA with Dunnett's multiple comparisons test; ** $p \leq 0.01$.

Our results demonstrated that HE-10-induced cytotoxicity can also occur independently of light exposure, as evidenced by the comparable increases in intracellular RONS with or without light. This finding suggests that HE-10 induces oxidative stress within VH10 cells regardless of lighting conditions. However, it's important to note that we measured HE-10 RONS-dependent H_2DCF oxidation 18 hours following exposures to estimate the long-term safety of the treatment. The adaptive mechanisms, as illustrated by autophagy upregulation (Fig. 6), may explain the lack of statistical differences between light and dark groups in long-term RONS measurements. Still, the short-time treatments caused statistically significant increases in NO (as documented by applying a DAF probe in Figure 9) only in light-unexposed HE-10-treated cells. The plausible explanation would be NO depletion through reaction with photoinduced $O_2^{\cdot -}$ generation in light-exposed cells. The generated peroxynitrite can account for a significant influence on cell cycle progression and autophagy upregulation. However, these propositions still need to be tested. The limitation in our experimental design highlights the need for more time-resolved studies to fully understand the dynamics of RONS generation and cellular responses to HE-10 treatment.

We observed the concentration-dependent cytotoxicity and enhanced effect under light conditions align with the known roles of NO in skin defense, wound healing, and tissue repair (Avci et al. 2013). However, the absence of a significant increase in intracellular NO production under light exposure at higher concentrations was unexpected and underscores the complexity of the reactive species generation dynamics. We decided to investigate the NO depletion mechanism in the light group using free radical inhibitors, but due to certain limitations, we were unable to conduct these experiments. Moreover, a study revealed that fluorescence increases in DAF-2 DA-loaded cells were observed only when NO-containing buffer was added directly, with a minimum detectable NO concentration of 7.7 μM, suggesting that DAF-2 DA's sensitivity may not be sufficient for detecting lower levels of NO production in cells (Roychowdhury et al. 2002). Yet, a mild increase in the detected NO levels even at 3 μM concentration indicates that HE-10 can act as a spontaneous NO releaser at low concentrations without causing tissue damage.

The G2/M checkpoint is a critical regulatory juncture within the cell cycle, inhibiting the transition into mitosis in the presence of genomic DNA damage (Löbrich and Jeggo 2007). The flow cytometric data indicate that the HE-10 complex increased accumulation of VH10 cells in the G2/M phase of the cell cycle, concomitantly with an

upregulation of the cyclin-dependent kinase inhibitor p21, while concurrently reducing the proportion of cells in the G1 phase upon light irradiation, especially at the higher concentrations. These results suggest that HE-10 exerts an inhibitory effect on cell cycle distribution, a finding that may have profound implications for processes such as tissue regeneration, wherein regulated cellular proliferation is essential (Zhu et al. 2002). As mentioned above, HE-10 induces the generation of RONS, which can cause DNA damage and subsequent apoptotic cell death. However, Ru complexes with similar cytotoxic properties accompanied by G2/M cell cycle arrest have recently been introduced as promising anticancer agents (Martin et al. 2014; De Grandis et al. 2021; Sun et al. 2021).

Basal concentrations of ROS are known to function as signaling molecules that facilitate cellular proliferation. In contrast, elevated ROS levels can inflict damage upon critical cellular components (Schieber and Chandel 2014). However, this might have a beneficial effect in terms of killing bacteria or cancer cells, as Ru complexes have shown promising efficacy against both (Weng et al. 2021; Navale et al. 2023). Our findings suggest that HE-10 induces elevated ROS levels, which might have a beneficial effect in terms of killing bacteria or cancer cells. However, we did not directly compare the effects of HE-10 on healthy skin cells versus skin disease models (Sarama et al. 2022). Therefore, we recommend conducting studies in *in vitro* and *in vivo* skin disease models to better understand the therapeutic potential of HE-10.

The observed enhanced cytotoxicity of HE-10 under light conditions suggests a degree of phototoxicity. While phototoxicity is often considered a safety concern for drugs and chemicals, it can be advantageous in certain therapeutic applications, such as photodynamic therapies (PDTs) for cancer or antimicrobial treatments (Harrison et al. 2023). Although our study focused on a Ru-NO complex, it's worth noting that Ru complexes lacking NO ligands have also shown promise as photosensitizers in PDTs (Le Gall et al. 2018). Photosensitizers typically operate through two types of photochemical reactions. In type-I photochemical reactions, the photosensitizers in the triplet excited state ($^3PS^*$) react directly with cellular components while forming ROS such as superoxide ions and hydroxyl radicals (Inguscio et al. 2012). In type-II photochemical reaction, the $^3PS^*$ mediates the generation of a highly toxic activated oxygen molecule, the singlet oxygen ($^1O_2$). In particular, Ru complexes mainly undergoing type-I photochemical reactions triggering superoxide generation have shown a prominent anticancer effect over the type-II photosensitizing complexes (Zhang et al. 2020). While we did not specifically investigate the photochemical reaction type for HE-10, the observed increase in RONS production and enhanced cytotoxicity under light conditions suggest that our compound may be undergoing similar photochemical processes.

The stability of Ru complexes is a critical determinant of their efficacy in medical applications. In this study, we used DMSO to dissolve the HE-10 complex, which was subsequently added to the cell culture media to establish different treatment concentrations. Our findings revealed that despite being stable in pure solvents and as a solid in the dark, this complex failed to maintain stability in the cell culture media and underwent spontaneous NO release throughout an incubation period of 18 hours at 37°C, especially under dark conditions. This observation indicates the occurrence of solvolysis when the complex was dissolved in the cell media, which is a limitation for potential therapeutic applications. This limitation can be eliminated through the development of drug delivery systems.

In conclusion, our study demonstrated that the Ru-NO complex HE-10 causes dose-dependent cytotoxicity in VH10 human fibroblast cells, with greater effects under light conditions at a low micromolar range of concentrations. This cytotoxicity is linked to oxidative stress and DNA damage, leading to changes in cell cycle distribution and apoptosis. Given its potential therapeutic application as a cytotoxic drug and photosensitizer in PDTs, the question of the cytotoxic selectivity of HE-10 toward cancer cells or bacteria remains to be answered. Although we confirmed a mild spontaneous enhancing effect of HE-10 on intracellular NO levels, the combination with white light had rather a negative impact on its NO elevating function.

This study will be crucial in determining the potential of HE-10 as a topical therapeutic agent for skin aging or diseases and in guiding the development of next-generation Ru-NO complexes for dermatological applications.

Conflict of interest. The authors declare that they have no conflict of interest.

Author contributions. HÖ collected, analyzed and interpreted the data, and prepared the manuscript for publication. HME performed and analyzed compound synthesis-related experiments, and wrote the related part of the manuscript. LR and MS helped design the study and supervised the data collection. MS and LR supervised the work and edited the manuscript. All authors have read and approved the final manuscript.

Funding statement. This study has received funding from the European Union's Horizon 2020 research and innovation program under the Marie Skłodowska-Curie grant agreement No. 813920, APVV-18-0336, and VEGA 2/0060/24.

Acknowledgment. I would like to express my sincere gratitude to my supervisor, Dr. Eliyahu Dremencov, for his encouragement and support in writing this article. I am grateful for his mentorship and positive influence throughout this process.

References

Avci P, Gupta A, Sadasivam M, Vecchio D, Pam Z, Pam N, Hamblin MR (2013): Low-level laser (light) therapy (LLLT) in skin: stimulating, healing, restoring. Semin. Cutan. Med. Surg. **32,** 41

Barbosa MI, Corrêa RS, Guedes AP, Graça AM, Andrade FM, Leite CM, Silveira-Lacerda EP, Ellena J, Reis HV, Doriguetto AC (2023): Nitrosyl/diphenylphosphine/amino acid-ruthenium complexes as inhibitors of MDA-MB-231 breast cancer cells. Inorganics **11,** 270
https://doi.org/10.3390/inorganics11070270

Bhowmik R, Roy M (2024): Recent advances on the development of NO-releasing molecules (NORMs) for biomedical applications. Eur. J. Med. Chem. **15,** 116217
https://doi.org/10.1016/j.ejmech.2024.116217

Bonnet S (2023): Ruthenium-based photoactivated chemotherapy. J. Am. Chem. Soc. **145,** 23397-23415
https://doi.org/10.1021/jacs.3c01135

Bruch-Gerharz D, Ruzicka T, Kolb-Bachofen V (1998): Nitric oxide in human skin: current status and future prospects. J. Invest. Dermatol. **110,** 1-7
https://doi.org/10.1046/j.1523-1747.1998.00084.x

Calabrese V, Mancuso C, Calvani M, Rizzarelli E, Butterfield DA, Giuffrida Stella AM (2007): Nitric oxide in the central nervous system: neuroprotection versus neurotoxicity. Nat. Rev. Neurosci. **8,** 766-775
https://doi.org/10.1038/nrn2214

Cheung A, Newland PL, Zaben M, Attard GS, Gray WP (2012): Intracellular nitric oxide mediates neuroproliferative effect of neuropeptide y on postnatal hippocampal precursor cells. J. Biol. Chem. **287,** 20187-20196
https://doi.org/10.1074/jbc.M112.346783

Csekes E, Vágvölgyi M, Hunyadi A, Račková L (2020): Protoflavones in melanoma therapy: Prooxidant and pro-senescence effect of protoapigenone and its synthetic alkyl derivative in A375 cells. Life Sci. **260,** 118419
https://doi.org/10.1016/j.lfs.2020.118419

Dai Z, Yu Z, Bai Y, Li J, Peng J (2021): Cobalt bis (2-ethylhexanoate) and terpyridine derivatives as catalysts for the hydrosilylation of olefins. Applied Organometallic Chemistry **35,** e6027
https://doi.org/10.1002/aoc.6027

De Grandis RA, Oliveira KM, Guedes AP, Dos Santos PW, Aissa AF, Batista AA, Pavan FR (2021): A novel ruthenium (II) complex with lapachol induces G2/M phase arrest through aurora-B kinase down-regulation and ROS-mediated apoptosis in human prostate adenocarcinoma cells. Front. Oncol. **11,** 682968
https://doi.org/10.3389/fonc.2021.682968

De La Cruz C, Sheppard N (2011): A structure-based analysis of the vibrational spectra of nitrosyl ligands in transition-metal coordination complexes and clusters. Spectrochim. Acta A Mol. Biomol. Spectrosc. **78,** 7-28
https://doi.org/10.1016/j.saa.2010.08.001

de Lima RG, Sauaia MG, Bonaventura D, Tedesco AC, Bendhack LM, da Silva RS (2006): Influence of ancillary ligand L in the nitric oxide photorelease by the [Ru (L)(tpy) NO] 3+ complex and its vasodilator activity based on visible light irradiation. Inorganica Chimica Acta **359,** 2543-2549
https://doi.org/10.1016/j.ica.2006.02.020

de Lima RG, Tedesco AC, da Silva RS, Lawrence MJ (2017): Ultradeformable liposome loaded with zinc phthalocyanine and [Ru (NH. NHq)(tpy) NO] 3+ for photodynamic therapy by topical application. Photodiagnosis Photodyn. Ther. **19,** 184-193
https://doi.org/10.1016/j.pdpdt.2017.05.013

de Souza Gois RG, Boffo EF, Júnior JCT, Andriani KF, Caramori GF, de Jesus Gomes A, Doro FG (2019): A ruthenium nitrosyl cyclam complex with appended anthracenyl fluorophore. Polyhedron **173,** 114117
https://doi.org/10.1016/j.poly.2019.114117

do Nascimento NRF, de Aguiar FLN, Santos CF, Costa AML, de Jesus Hardoim D, da Silva Calabrese K, Almeida-Souza F, de Sousa EHS, de França Lopes LG, Teixeira MJ (2019): In vitro and in vivo leishmanicidal activity of a ruthenium nitrosyl complex against Leishmania (Viannia) braziliensis. Acta Trop. **192,** 61-65
https://doi.org/10.1016/j.actatropica.2019.01.021

Dusting G (1995): Nitric oxide in cardiovascular disorders. J. Vasc. Res. **32,** 143-161
https://doi.org/10.1159/000159089

Elbeheiry HM, Schulz M (2024): Direct and indirect approaches to red-shift photoactivated nitric oxide release. Coordination Chemistry Reviews **515,** 215921
https://doi.org/10.1016/j.ccr.2024.215921

Fry NL, Wei J, Mascharak PK (2011): Triggered dye release via photodissociation of nitric oxide from designed ruthenium nitrosyls: turn-ON fluorescence signaling of nitric oxide delivery. Inorg. Chem. **50,** 9045-9052
https://doi.org/10.1021/ic201242d

Guzik T, Korbut R, Adamek-Guzik T (2003): Nitric oxide and superoxide in inflammation. J. Physiol. Pharmacol. **54,** 469-487

Harrison TJ, Chen X, Yasoshima K, Bauer D (2023): Phototoxicity - medicinal chemistry strategies for risk mitigation in drug discovery. J. Med. Chem. **66,** 9345-9362
https://doi.org/10.1021/acs.jmedchem.3c00749

Honari G (2017): Skin structure and function. In: Sensitive Skin Syndrome (Ed. G Honari, R Andersen, HL Maibach) pp. 16-22, Boca Raton
https://doi.org/10.1201/9781315121048-3

Inguscio V, Panzarini E, Dini L (2012): Autophagy contributes to the death/survival balance in cancer photodynamic therapy. Cells **1,** 464-491
https://doi.org/10.3390/cells1030464

Ji CH, Kwon YT (2017): Crosstalk and interplay between the ubiquitin-proteasome system and autophagy. Mol. Cells **40,** 441-449
https://doi.org/10.14348/molcells.2017.0115

Kajiya K, Huggenberger R, Drinnenberg I, Ma B, Detmar M (2008): Nitric oxide mediates lymphatic vessel activation via soluble guanylate cyclase α1β1-impact on inflammation. FASEB J. **22,** 530-537
https://doi.org/10.1096/fj.07-8873com

Kim JH, Choi MS (2023): Nitric oxide signal transduction and its role in skin sensitization. Biomol. Ther. **31,** 388
https://doi.org/10.4062/biomolther.2023.101

Kumar R, Kumar S, Bala M, Ratnam A, Singh U, Ghosh K (2018): Unprecedented oxidation of aldimine to carboxamido function during reactivity studies on ruthenium complex with acidified

nitrite solution: Synthesis of ruthenium nitrosyl complex having {RuNO} 6 moiety and photorelease of coordinated NO. Journal of Organometallic Chemistry **863,** 77-83
https://doi.org/10.1016/j.jorganchem.2018.02.010

Lavnikova N, Laskin DL (1995): Unique patterns of regulation of nitric oxide production in fibroblasts. J. Leucoc. Biol. **58,** 451-458
https://doi.org/10.1002/jlb.58.4.451

Le Gall T, Lemercier G, Chevreux S, Tücking KS, Ravel J, Thétiot F, Jonas U, Schönherr H, Montier T (2018): Ruthenium (II) polypyridyl complexes as photosensitizers for antibacterial photodynamic therapy: A structure-activity study on clinical bacterial strains. Chem. Med. Chem. **13,** 2229-2239
https://doi.org/10.1002/cmdc.201800392

Löbrich M, Jeggo PA (2007): The impact of a negligent G2/M checkpoint on genomic instability and cancer induction. Nat. Rev. Cancer **7,** 861-869
https://doi.org/10.1038/nrc2248

Man MQ, Wakefield JS, Mauro TM, Elias PM (2022): Role of nitric oxide in regulating epidermal permeability barrier function. Exp. Dermatol. **31,** 290-298
https://doi.org/10.1111/exd.14470

Marquele-Oliveira F, de Almeida Santana DC, Taveira SF, Vermeulen DM, de Oliveira ARM, da Silva RS, Lopez RFV (2010): Development of nitrosyl ruthenium complex-loaded lipid carriers for topical administration: improvement in skin stability and in nitric oxide release by visible light irradiation. J. Pharm. Biomed. Anal. **53,** 843-851
https://doi.org/10.1016/j.jpba.2010.06.007

Martin A, Byrne A, Burke CS, Forster RJ, Keyes TE (2014): Peptide-bridged dinuclear Ru (II) complex for mitochondrial targeted monitoring of dynamic changes to oxygen concentration and ROS generation in live mammalian cells. J. Am. Chem. Soc. **136,** 15300-15309
https://doi.org/10.1021/ja508043q

Mowbray M, McLintock S, Weerakoon R, Lomatschinsky N, Jones S, Rossi AG, Weller RB (2009): Enzyme-independent NO stores in human skin: quantification and influence of UV radiation. J. Invest. Dermatol. **129,** 834-842
https://doi.org/10.1038/jid.2008.296

Navale GR, Singh S, Ghosh K (2023): NO donors as the wonder molecules with therapeutic potential: Recent trends and future perspectives. Coordination Chemistry Reviews **481,** 215052
https://doi.org/10.1016/j.ccr.2023.215052

Rose MJ, Mascharak PK (2008): Photoactive ruthenium nitrosyls: Effects of light and potential application as NO donors. Coordination Chemistry Reviews **252,** 2093-2114
https://doi.org/10.1016/j.ccr.2007.11.011

Roychowdhury S, Luthe A, Keilhoff G, Wolf G, Horn TF (2002): Oxidative stress in glial cultures: detection by DAF-2 fluorescence used as a tool to measure peroxynitrite rather than nitric oxide. Glia **38,** 103-114
https://doi.org/10.1002/glia.10024

Sarama R, Matharu PK, Abduldaiem Y, Corrêa MP, Gil CD, Greco KV (2022): In vitro disease models for understanding psoriasis and atopic dermatitis. Front. Bioeng. Biotechnol. **10,** 803218
https://doi.org/10.3389/fbioe.2022.803218

Schieber M, Chandel NS (2014): ROS function in redox signaling and oxidative stress. Curr. Biol. **24,** R453-R462
https://doi.org/10.1016/j.cub.2014.03.034

Shi S-W, Li Y-H, Zhang Q-L, Yang S-P, Liu J-G (2019): Targeted and NIR light-controlled delivery of nitric oxide combined with a platinum (IV) prodrug for enhanced anticancer therapy. J. Mater. Chem. B **7,** 1867-1874
https://doi.org/10.1039/C8TB02743A

Singh S, Chaudhary PK, Prasad R, Singh U, Ghosh K (2024): Visible light induced generation of nitric oxide from designed ruthenium nitrosyl complex and studies on antibacterial activity. Journal of Molecular Structure **1310,** 138323
https://doi.org/10.1016/j.molstruc.2024.138323

Stadler E, Eibel A, Fast D, Freißmuth H, Holly C, Wiech M, Moszner N, Gescheidt G (2018): A versatile method for the determination of photochemical quantum yields via online UV-Vis spectroscopy. Photochem. Photobiol. Sci. **17,** 660-669
https://doi.org/10.1039/c7pp00401j

Stepanenko I, Zalibera M, Schaniel D, Telser J, Arion VB (2022): Ruthenium-nitrosyl complexes as NO-releasing molecules, potential anticancer drugs, and photoswitches based on linkage isomerism. Dalton Trans. **51,** 5367-5393
https://doi.org/10.1039/D2DT00290F

Stunova A, Vistejnova L (2018): Dermal fibroblasts - A heterogeneous population with regulatory function in wound healing. Cytokine Growth Factor Rev. **39,** 137-150
https://doi.org/10.1016/j.cytogfr.2018.01.003

Sun Q, Li Y, Shi H, Wang Y, Zhang J, Zhang Q (2021): Ruthenium complexes as promising candidates against lung cancer. Molecules **26,** 4389
https://doi.org/10.3390/molecules26154389

Suschek CV, Feibel D, von Kohout M, Opländer C (2022): Enhancement of nitric oxide bioavailability by modulation of cutaneous nitric oxide stores. Biomedicines **10,** 2124
https://doi.org/10.3390/biomedicines10092124

Thangaraju P, Varthya SB (2022): ISO 10993: Biological evaluation of medical devices. In: Medical Device Guidelines and Regulations Handbook. (Ed. PST Shanmugam, P Thangaraju, N Palani, T Sampath), pp. 163-187, Springer Nature Switzerland
https://doi.org/10.1007/978-3-030-91855-2_11

Tobin DJ (2017): Introduction to skin aging. J. Tissue Viability **26,** 37-46
https://doi.org/10.1016/j.jtv.2016.03.002

Wagner RN, Piñón Hofbauer J, Wally V, Kofler B, Schmuth M, De Rosa L, De Luca M, Bauer JW (2021): Epigenetic and metabolic regulation of epidermal homeostasis. Exp. Dermatol. **30,** 1009-1022
https://doi.org/10.1111/exd.14305

Walton DM, Minton SD, Cook AD (2019): The potential of transdermal nitric oxide treatment for diabetic peripheral neuropathy and diabetic foot ulcers. Diabetes Metab. Syndr. **13,** 3053-3056
https://doi.org/10.1016/j.dsx.2018.07.003

Weller R (2003): Nitric oxide donors and the skin: useful therapeutic agents? Clin. Sci. **105,** 533-535
https://doi.org/10.1042/CS20030241

Weng C, Shen L, Teo JW, Lim ZC, Loh BS, Ang WH (2021): Targeted antibacterial strategy based on reactive oxygen species

generated from dioxygen reduction using an organoruthenium complex. JACS Au **1,** 1348-1354
https://doi.org/10.1021/jacsau.1c00262

Works CF, Ford PC (2000): Photoreactivity of the ruthenium nitrosyl complex, Ru (salen)(Cl)(NO). Solvent effects on the back reaction of NO with the lewis acid RuIII (salen)(Cl). J. Am. Chem. Soc. **122,** 7592-7593
https://doi.org/10.1021/ja000137p

Yaşayan G, Nejati O, Ceylan AF, Karasu Ç, Ugur PK, Bal-Öztürk A, Zarepour A, Zarrabi A, Mostafavi E (2023): Tackling chronic wound healing using nanomaterials: advancements, challenges, and future perspectives. Applied Materials Today **32,** 101829
https://doi.org/10.1016/j.apmt.2023.101829

Zhang X, Huang X, Xie A, Zhang X, Deng J, Zou D, Zou J (2020): Boosting type I process of Ru (II) compounds by changing tetrazole ligand for enhanced photodynamic therapy against lung cancer. J. Inorg. Biochem. **212,** 111236
https://doi.org/10.1016/j.jinorgbio.2020.111236

Zhu X, Di Y, Hu C, Wang Z (2002): Expression of positive and negative regulators of cell cycle during wound healing. Chin. Med. J. **115,** 326-330

Received: June 23, 2024
Final version accepted: July 19. 2024